Spin-ordering mediated orbital hybridization in CoO at high pressures

Yang Ding,[1,*] Javier Fernandez-Rodriguez,[1,2] Jungho Kim,[1] Fangfei Li,[3] Diego Casa,[1] Mary Upton,[1] Thomas Gog,[1] Ho-kwang Mao,[3,4] and Michel van Veenendaal[1,2]

[1]*Advanced Photon Source, Argonne National Laboratory, 9700 S. Cass Avenue, Argonne, Illinois 60439, USA*

[2]*Department of Physics, Northern Illinois University, DeKalb, Illinois 60115, USA*

[3]*HPSynC, Geophysical Laboratory, Carnegie Institution of Washington, Argonne, Illinois 60439, USA*

[4]*Geophysical Laboratory, Carnegie Institution of Washington, 5251 Broad Branch Road N.W., Washington, DC 20015, USA*

(Received 12 April 2012; revised manuscript received 3 August 2012; published 10 September 2012)

We demonstrate a strong dependence of high-resolution $1s3p$ (or K_β) resonant x-ray emission spectroscopy (RXES) on local spin correlations at high pressure. We show that the pre-edge region in K_β RXES of CoO can be separated into a local quadrupolar contribution and nonlocal dipolar intensity, which arises from the mixing of cobalt $4p$ states with neighboring cobalt $3d$ orbitals. For pressures of 0–12 GPa, we observe a twofold increase in nonlocal contributions with respect to local contributions. For pressures greater than 12 GPa, the ratio remains nearly constant. The observed pressure dependence and strong intensity changes cannot be explained by a conventional picture of bond-length shortening and is ascribed to increased intersite $4p$-$3d$ mixing due to changes in magnetic ordering. These results are supported by theoretical calculations.

DOI: 10.1103/PhysRevB.86.094107 PACS number(s): 62.50.−p, 75.30.−m, 78.70.En

I. INTRODUCTION

In the Mott insulators, the charge fluctuations are strongly suppressed due to the on-site Coulomb interactions, which results in the $3d$ electrons showing both localized and delocalized behaviors.[1] The competition between localization and delocalization, i.e., the interplay between electron correlations and intersite orbital hybridization in low-lying electronic structures, accounts for many elementary excitations that determine the transport, magnetic, and electronic properties of $3d$ transition-metal compounds.[2–4] Understanding such duality of the $3d$ electrons is central to the physics of $3d$ transition-metal compounds. Core-level x-ray spectroscopic methods are the extensively applied means for studying the dynamics of $3d$ electrons. However, despite the advances made in theory and experiments[5–15] over the last two decades, it still remains a challenge to apply them to study the nonlocal excitations, which could be associated with the delocalized behaviors of $3d$ electrons (such as intersite orbital hybridization and spin ordering). That is because it is difficult to conclusively identify the nonlocal excitations without directly observing how they form and evolve in the core-level x-ray spectra.

To further explore this subject, we integrated the recently emerging high-resolution resonant x-ray emission spectroscopy (RXES) technique[4,16] with high-pressure environment to study nonlocal transitions arising from intersite hybridization in CoO. CoO is a prototype Mott insulator that displays very little intersite hybridization under ambient conditions.[13] Our motivation is that the nonlocal transitions are sensitive to changes in nearest-neighbor correlation functions,[17] which can be tuned by an external pressure. Therefore the nonlocal transitions should show the pressure dependent changes, while the local excitations will not show such changes. This could enable us to directly identify the nonlocal excitations from the local excitation in the RXES spectra. In this paper, we report high-resolution $1s3p$ RXES measurements on CoO at pressures of up to 28 GPa. We focus on the pre-edge features and demonstrate that they can be separated into local quadrupolar and nonlocal dipolar intensities. The nonlocal contribution occurs due to the mixing of $4p$ states with neighboring cobalt $3d$ orbitals. Although this mixing is weak, due to strong dipolar matrix elements, the intensity is comparable to that of quadrupolar transitions. Moreover, because nonlocal features only exist by virtue of the coupling to neighboring sites, they are sensitive to changes in nearest-neighbor correlation functions. In our study, the relative intensities of nonlocal and local RXES increased by a factor of 2 as the pressure increased from 0 to 12 GPa, after which it became nearly constant. This pressure dependence is impossible to attribute to bond length shortening (which is equal to 1.9% at 12 GPa) but is in good agreement with an increase in nonlocal intensity due to changes in nearest-neighbor spin correlations.

II. EXPERIMENT

High-pressure experiments were performed with Mao-type panoramic high-pressure cells.[18] CoO polycrystalline samples (99.99% purity), which were purchased from Sigma-Aldrich, were loaded with ruby chips (as a pressure standard) into an approximately 150-μm-diameter hole in a beryllium metal gasket. The pressures were determined by ruby fluorescence. RXES measurements were performed at the 30-ID and 9-ID beamlines of the Advanced Photon Source (APS) at Argonne National Laboratory (ANL) (a detailed description of these instruments can be found elsewhere[19]). Incident x rays from two APS undulators were monochromatized by high-heat load monochromators and high-resolution monochromators, which were then focused at the sample position. The incident energy was calibrated with a standard Co foil at the K-edge absorption inflection point at 7709 eV. X-ray fluorescence emitted from the sample was analyzed with a Ge(444) spherically diced analyzer on a 1-m Rowland-circle spectrometer. The sample scattering plane was horizontal. The overall energy resolution

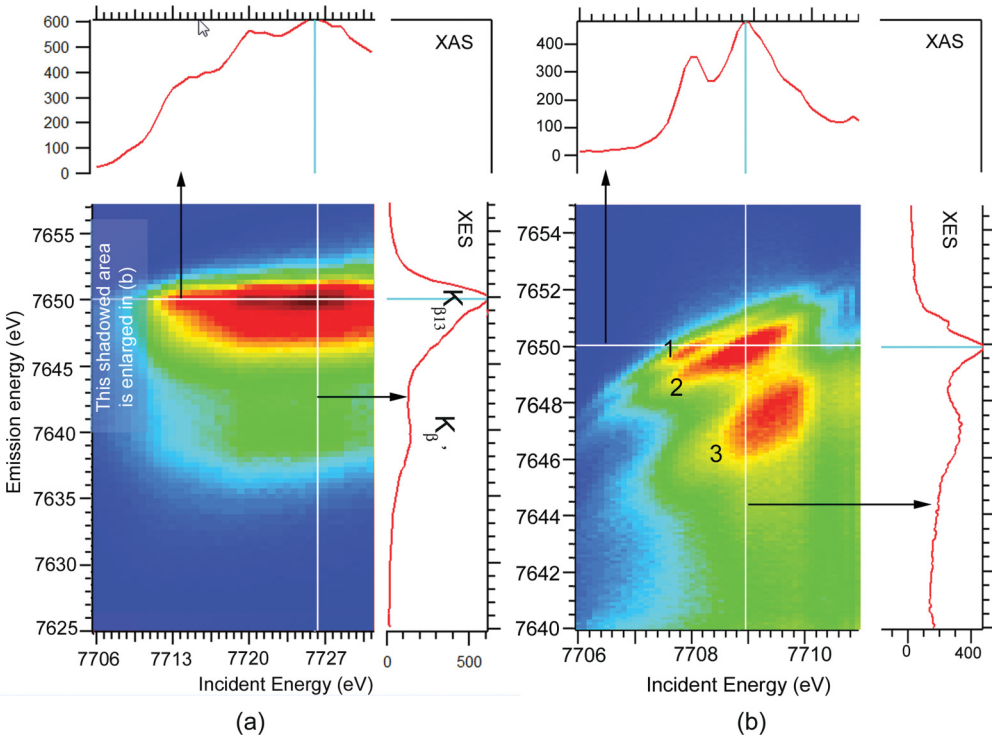

FIG. 1. (Color online) High-pressure $1s3p$ RXES map of CoO at 12 GPa. (a) The RXES map was created at emission energies ranging from 7625 to 7657 eV and incident energies ranging from 7706 to 7713 eV. The energy scanning step size was 1 eV. (b) The enlarged REXS map from (a) at emission energies ranging from 7640 to 7654 eV and incident energies ranging from 7706 to 7711 eV. The energy scanning step size was 0.2 eV. The line spectra in (a) and (b) on the top represent the partial yield fluoresce x-ray-absorption spectrum, while the spectra on the left are emission spectra. The three peaks labeled 1, 2, and 3 show the Raman shift due to resonance effects.

was estimated from the full width at half maximum (FWHM) of the elastic peak, and a value of 0.16 eV was obtained at the emission energy of Co $K_{\beta 13}$ (7650 eV). For the high-pressure RXES measurements, the diamond-anvil cell was set to allow both incident and emitted x rays to penetrate the Be gasket window. RXES spectra were obtained by scanning the analyzer for emission spectra in the region of the Co K_β emission peak while varying the incident energy around the Co K absorption-edge region. Because this type of RXES measurement involves two electronic transitions, including an excitation from $1s$ to $4p$ (or $3d$) followed by a decay from $3p$ to $1s$, it is called $1s3p$ RXES or K_β RXES. RXES data collected at 12 GPa are plotted in Fig. 1. For further analysis, RXES data are also plotted as the incident energy versus energy transfer (the energy difference between incident and emission energy) and interpolated on a grid with a step size of 0.01 eV (Fig. 2). High-pressure RXES measurements were repeated several times and were performed under both nonhydrostatic compression conditions without a pressure medium and nearly hydrostatic compression conditions with silicone oil as the pressure medium. The highest pressure used in these measurements was approximately 28 GPa.

III. RESULTS AND ANALYSIS

As shown in Fig. 1, when the incident energy was greater than the Co K absorption edge (7709 eV) [Fig. 1(a)], only two nonresonant emission peaks, $K_{\beta 13}$ and K_β, were observed in the map. When the incident energy was tuned to the Co K absorption edge, three resonant peaks [labeled as 1, 2, and 3 in Fig. 1(b)] appeared in the map, and their positions shifted with the incident energy (Raman shifts due to the resonance effect). To investigate how these resonant peaks change with pressure, we collected $1s3p$ RXES data on CoO and Co_3O_4 up to 28 GPa, and selected results are plotted in Fig. 2.

Peak 3 exhibited a sizable increase in intensity from low to high pressure, while peaks 1 and 2 remained nearly constant. To quantitatively characterize the change in peaks, the pressure dependent intensity ratio of peak 3 to peak 2 was plotted (Fig. 3) based on data obtained from nearly hydrostatic and nonhydrostatic compression measurements. As shown in Fig. 2, the intensity ratio almost doubled from 0.55 (at 3.3 GPa) to approximately 1.0 (at 12.5 GPa) in the nearly hydrostatic compression measurements and increased by approximately 26% from 0.53 (at 0.2 GPa) to 0.67 (at 12.3 GPa) in the nonhydrostatic compression measurements. However, at pressures greater than approximately 12 GPa, the ratio was nearly constant. The background from the Be gasket at each pressure point was collected. Structural and pressure dependences were not significant, contributing less than 1% to each set of RXES data, which indicated that the change in peak 3 was an intrinsic transition of the CoO system. For comparison, Co_3O_4, which has no magnetic ordering at high pressure but features resonant peaks similar to those of

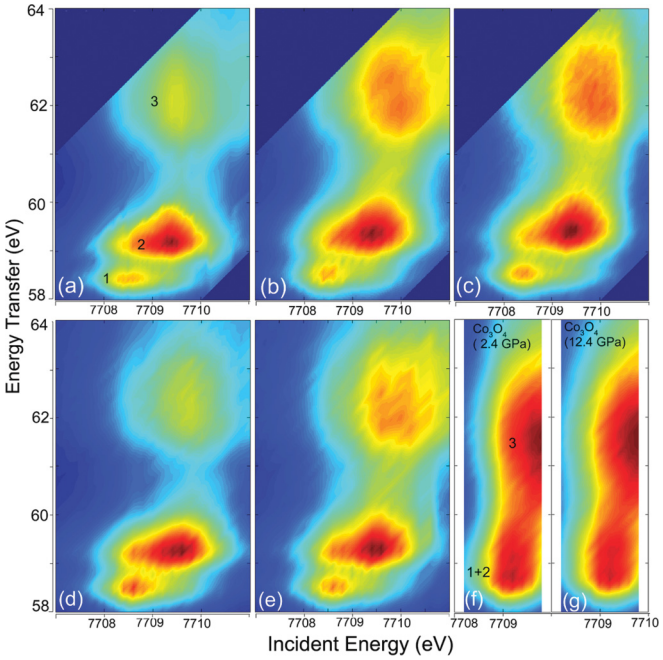

FIG. 2. (Color online) RXES data were plotted as the incident energy versus energy transfer. The peaks labeled 1, 2, and 3 correspond to the three peaks in Fig. 1. (a), (b), and (c) are RXES data collected on CoO at 0.2, 12, and 28 GPa, respectively, in the absence of a medium. (d) and (e) are RXES data collected at 3.3 and 6 GPa on CoO with Si oil as the medium. (f) and (g) are the RXES data collected on Co_3O_4 at 2.4 and 12.4 GPa, respectively, with Si oil as the medium.

CoO, was chosen as a reference system [Figs. 2(f) and 2(g)]. Compared with CoO, similar changes were not observed in Co_3O_4 at pressures up to 14 GPa.

To understand the underlying mechanism of this transition, we analyzed the RXES data by calculating the cross section

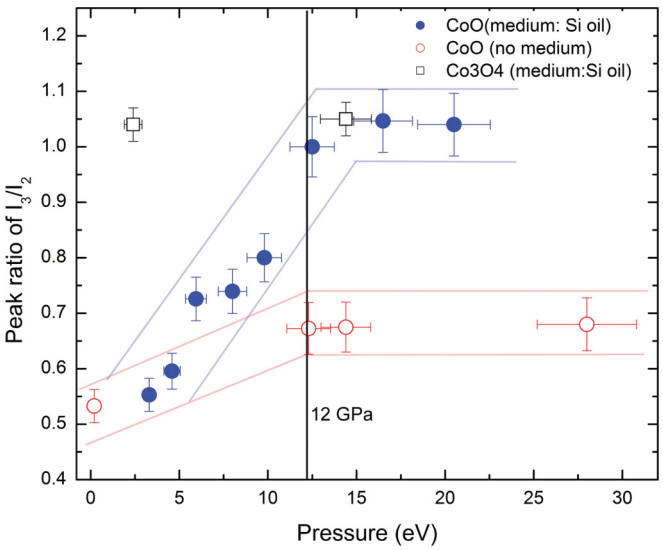

FIG. 3. (Color online) The pressure-dependent intensity ratio (I_3/I_2) of peak 3 and peak 2 (as labeled in Figs. 1 and 2). The blue and red lines are plotted to show the trend of changes.

TABLE I. Model parameters used in the CoO_6 cluster calculation of the RIXS spectra in CoO.

Parameters	Values (eV)
Racah A	5.2
Racah B	0.14
Racah C	0.54
Δ	5.5
$pd\sigma$	1.3
$pd\pi$	−0.6
$pp\sigma$	0.55
$pp\pi$	−0.15
$10\,Dq$	0.7

$F(\omega,\omega')$ using the Kramers-Heisenberg formula:[12]

$$F(\omega,\omega') = \sum_f \left| \sum_n \frac{\langle f|T|n\rangle\langle n|T|g\rangle}{E_g - E_n + \omega + i\frac{\Gamma_n}{2}} \right|^2 \times \frac{\Gamma_f}{2\pi} \frac{1}{(E_g - E_f + \omega - \omega')^2 + \frac{\Gamma_f^2}{4}}, \quad (1)$$

where ground (g), intermediate (n), and final (f) state electron wave functions have energies of E_g, E_n, and E_f, respectively; Γ_n and Γ_f are the intermediate- and final-state lifetime broadenings, respectively; and T is the electric-multipole transition operator. The difference between the incident and emitted x ray energy is the energy transfer or energy loss ($\omega - \omega'$).

We performed ligand-field multiplet calculations on a CoO_6^{10-} cluster in octahedral symmetry (O_h) to obtain the electronic states and RXES cross section.[8,20] The model included spin-orbit coupling, an external magnetic field, and on-site Coulomb interactions, as well as the full multiplet structure and coupling to the surrounding oxygen ligands. The ground, intermediate, and final states were diagonalized, and the cross section was calculated using Eq. (1). The parameters for spin-orbit coupling and Slater integrals (reduced at 80%) were calculated within the limits of Hartree-Fock. For the determination of the electrostatic crystal field ($10Dq$), hybridization and charge-transfer energies, the parameters given by van Elp *et al.*,[21] were applied and are also listed in Table I.

Let us first consider the local transitions. For the ground state, we considered the $3d^n$ and $3d^{n+1}\underline{L}$ configurations, where $n = 7$ for Co^{2+} and $\underline{L}$ denotes a hole in the neighboring O $2p$ ligands. Full shells were not included in this case. For the intermediate and final states, we included the $\underline{c}3d^{n+1}$ and $\underline{c}3d^{n+2}\underline{L}$ configurations, where $\underline{c}$ denotes a $1s$ and $3p$ core hole. Temperature effects were also taken into account for the lowest-lying states in ${}^4T_{1g}$. For lifetime broadening, 1.4 and 0.3 eV were used for the intermediate and final states, respectively. The parameters of the Hamiltonian were set according to the change in bond length due to the applied pressure, in accordance with Harrison's relations.[17]

The results of the simulations of $1s3p$ RXES including only local quadrupolar contributions at 1 bar and 12 GPa are displayed in Figs. 4(a) and 4(d). Clearly, feature 3 in the experimental RXES (Fig. 2) at an energy loss of 62 eV was not present in the simulation when only local transitions were

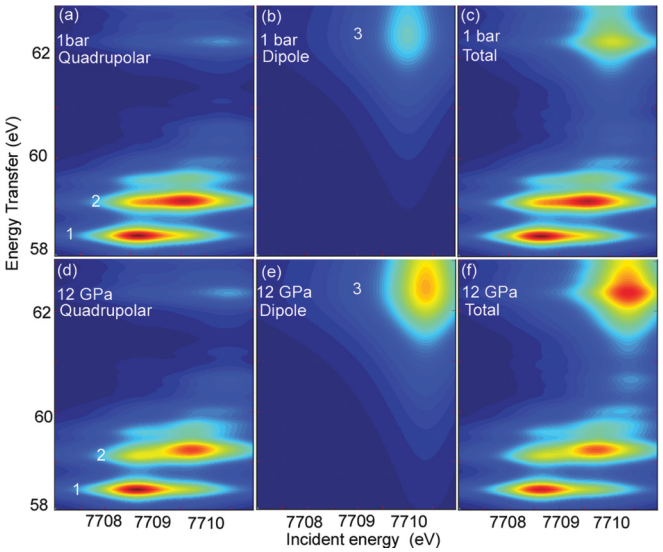

FIG. 4. (Color online) $1s3p$ RXES simulations of a CoO_6^{10-} cluster based on ligand-field multiplet calculations, which were performed considering both local quadrupolar transitions [(a) and (d)] and nonlocal dipolar excitations arising from intersite hybridization between on-site $4p$ and neighboring $3d$ orbitals [(b) and (e)]. (c) and (f) are the sums of local and nonlocal contributions.

considered in the modeling. Therefore we assigned feature 3 in Fig. 2 as the nonlocal contribution due to the mixing of $4p$ states with the $3d$ band. Note that these transitions are different from the quadrupolar excitations into the $3d$ band that appear at lower energy losses due to excitonic effects between the core hole and electrons excited into the $3d$ orbitals. Because nonlocal transitions occur in states with predominantly $3d$ character, they can be thought of as excitations into neighboring cobalt sites. Although this mixing is relatively small, the transitions are dipole allowed, and the intensity becomes comparable to that of weak quadrupolar features. Because these transitions only exist by virtue of coupling to neighboring cobalt sites, the spectral weight becomes sensitive to changes in coupling.

To calculate nonlocal intersite transitions, we considered the intermediate- and final-state configurations $\underline{c}3d^n(4p3d')^1$ and $\underline{c}3d^{n+1}\underline{L}(4p3d')^1$, with $\underline{c}$ representing $1s$ or $3p$ core holes and $(4p3d')$ representing the hybrid $4p$-$3d$ state with predominantly nonlocal $3d'$ character but excluding the $3d$ orbital on the site where the RXES process occurs. For final-state lifetime broadening, nonlocal dipolar transitions were set to 1.5 eV to take into account bandwidth effects. As shown in Figs. 4(b) and 4(e), the RXES process that includes nonlocal excitations provides additional spectral weight at an energy loss of approximately 62 eV. Finally, Figs. 4(c) and 4(f) present the simulated RXES based on both local quadrupolar and nonlocal dipole contributions, which show good agreement with the experimental data. These results indicate that peak 3 could not be attributed to coherent interference effects, as proposed in Ref. 13.

According to previous high-pressure x-ray[22] and neutron-diffraction experiments,[23] the lattice parameters continuously decrease with pressure, and anomalous changes do not occur at pressures below 40 GPa. Correspondingly, the bond length of Co-O decreases by approximately 1.9% from 2.13 Å (at 1 bar) to 2.09 Å (at 12 GPa).[22] This bond length reduction could only result in a 7% increase in $4p$-$3d$ intersite hybridization,[17] which cannot explain the twofold increase in the intersite transitions relative to the local transitions. Moreover, a reduction in bond length cannot explain why, after a continuous increase in the intersite RXES to 12 GPa, the ratio remains nearly constant for higher pressures. Furthermore, Co_3O_4, a system that has resonant peaks similar to those of CoO, exhibits no observable changes at pressures up to 14.4 GPa [Figs. 2(f) and 2(g)]. Therefore the evolution of the intersite RXES cannot be solely attributed to a reduction in bond length.

In addition to the change in bond length, CoO undergoes a pressure-induced paramagnetic (PM) to antiferromagnetic (AFM) ordering transition. According to neutron powder measurements,[22] the transition starts at 2.2 GPa in CoO, and the magnetic moment increases as the pressure increases to 9 GPa, the highest pressure that could be achieved for the neutron measurement. The relative orientation of the magnetic moments can influence the RXES due to exchange interactions between sites. An excited electron in the $4p$ state can only hybridize with the neighboring cobalt site when its spin is antiparallel to the Co magnetic moment. In NaCl-type structured CoO,[22,23] there are six neighboring Co ions that connect to the central Co ion through O at an angle of 180° [Fig. 5(d)]. In the lowest perturbation order, the mixing of the $4p$ orbital with the $3d$ band is of the order of $(t_\sigma/E_\sigma)^2$, where t_σ and E_σ are the effective hybridization and energy difference, respectively, between the $4p$ and $3d$ states, which depend on the spin (σ) of the excited $4p$ electron. The z direction of the spin is determined by the direction of the cobalt moment at the site of the RXES process. Because the intensity is dominated by dipolar transitions into the $4p$ orbital, the RXES intensity is directly proportional to this mixing. Let us first look at one possible effect of hybridization. The effective hybridizations can be written as $t_\uparrow = t\langle\sin(\theta_j/2)\rangle$ and $t_\downarrow = t\langle\cos(\theta_j/2)\rangle$ ($\uparrow$: spin up; $\downarrow$: spin down; and θ_j is the angle between neighboring spin directions). In the paramagnetic case, thermal averaging gives $t_\uparrow = t_\downarrow = t/2$. In contrast, in the antiferromagnatic state, $t_\uparrow = t$ and $t_\downarrow = 0$. Therefore changes in the effective mixing between $4p$ and $3d$ should not occur. However, a difference in E_σ is observed due to the exchange splitting of the $4p$ band. Defining Δ as the energy difference between the $\underline{c}3d^n4p^1(3d')^n$ and $\underline{c}3d^n(3d')^{n+1}$ configurations, we obtain $E_\uparrow = \Delta - J_H$ and $E_\downarrow = \Delta + J_H$, where J_H is the Hund's exchange between the $4p$ and $3d$ electrons on the site with the core hole. Thus the relative spectral weights in the antiferromagnetic versus the paramagnetic state are given by $2/[1 + (E_\uparrow/E_\downarrow)^2]$. This ratio approaches 2 in the limit $E_\downarrow \gg E_\uparrow$, which is in agreement with the results obtained in the nearly hydrostatic compression experiment. These results are shown schematically in Fig. 5. Clearly, if the coupling of the down spin approaches zero, then the mixing with the neighboring cobalt sites in the antiferromagnetic state is twice that in the paramagnetic state. When this change in the spectral weight of the nonlocal dipolar feature is included in the numerical calculations, the experimental spectra at 12 GPa are effectively simulated, as shown in Fig. 4(e). In nonhydrostatic compression, intersite mixing is significantly suppressed because uniaxial strain reduces spin ordering in

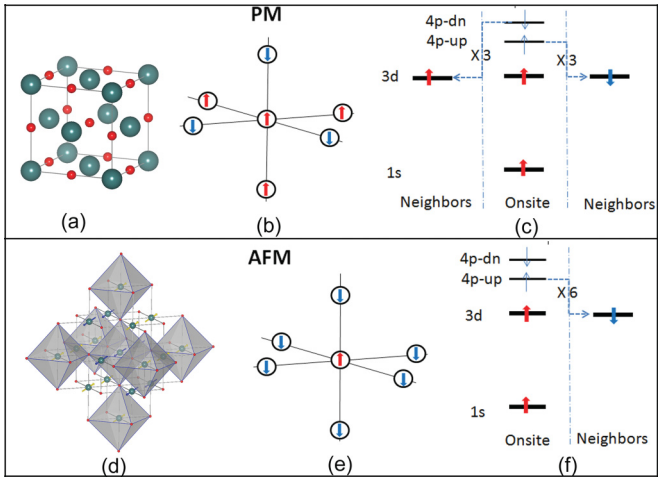

FIG. 5. (Color online) Schematic depiction of hybridization between the on-site $4p$ orbital and neighboring Co $3d$ orbital in the AFM and PM state.

CoO compared with that in nearly hydrostatic compression.[24] Once a PM-AFM transition begins in CoO, the mixing between the on-site $4p$ and neighboring $3d$ orbitals continuously increases until the spins are completely antiferromagnetically aligned. Therefore the lack of an increase in the RXES intensity of peak 3 at approximately 12 GPa suggests that the AFM moment is saturated and that AFM ordering is complete. In contrast, because Co_3O_4 has no such AFM spin transitions in this pressure range, intersite hybridization does not occur under compression, which provides additional evidence that spin ordering plays a role in the intersite hybridization of CoO. Currently, there are only two x-ray techniques available for studying AFM transitions at high pressure, including x-ray synchrotron Mössbauer and magnetic scattering. The former requires isotope-enriched samples, and the latter requires high-quality single crystals and provides weak signals. Therefore both probes have severe limitations in their application. Neutron diffraction, the best technique for studying magnetism, is presently limited to low-pressure regions (typically below 15 GPa). However, RXES is free of these limitations and could be applied to AFM transitions in various materials at pressures >100 GPa, thereby serving as a promising and unique probe for high-pressure magnetism research.

In addition, we need to point out that, as the spin-mediated $4p$-$3d$ intersite hybridization at high pressure is associated with the charge-transfer energy Δ and superexchange interaction strength, both of which could be changed by pressure, it remains interesting to determine which term plays a dominant role in the hybridization. This might be able to be determined by comparing results from high-pressure and low-temperature measurements, respectively.

IV. CONCLUSIONS

In summary, we discovered a strong dependence of high-resolution $1s3p$ RXES on local spin correlations in CoO at high pressure. This result not only affirms the evolution of $3d$-$4p$ intersite hybridization but also reveals the interesting role of spin ordering in intersite orbital hybridization in CoO at high pressure, which could serve as a new x-ray probe for studying AFM ordering transitions at high pressures.

ACKNOWLEDGMENTS

This research was based on work supported in part by EFree, an Energy Frontier Research Center funded by the US Department of Energy, Office of Science, and Office of Basic Energy Sciences (BES) under Award No. DE-SC0001057. Argonne is supported by US DOE Contract No. DE-AC02-6CH11357. The APS is supported by DOE-BES under Contract No. DE-AC02-06CH11357. The theory was supported by the US Department of Energy (DOE), Office of Basic Energy Sciences, Division of Materials Sciences and Engineering under Award No. DE-FG02-03ER46097, NIU's Institute for Nanoscience, Engineering, and Technology and by the ComputationalMaterials Science Network (CMSN) under grant DE-FG02-08ER46540.

*Author to whom correspondence should be addressed: yangding@aps.anl.gov

[1] E. Dagotto, Science **309**, 257 (2005).
[2] J. Zaanen, G. A. Sawatzky, and J. W. Allen, Phys. Rev. Lett. **55**, 418 (1985).
[3] P. A. Lee, Science **277**, 50 (1997).
[4] L. J. P. Ament, M. van Veenendaal, T. P. Devereaux, J. P. Hill, and J. van den Brink, Rev. Mod. Phys. **83**, 705 (2011).
[5] I. S. Elfimov, V. I. Anisimov, and G. A. Sawatzky, Phys. Rev. Lett. **82**, 4264 (1999).
[6] M. A. vanVeenendaal, H. Eskes, and G. A. Sawatzky, Phys. Rev. B **47**, 11462 (1993); M. A. vanVeenendaal and G. A. Sawatzky, *ibid.* **49**, 3473 (1994); K. Okada and A. Kotani, *ibid.* **52**, 4794 (1995).
[7] A. Shukla, M. Calandra, M. Taguchi, A. Kotani, G. Vankó, and S.-W. Cheong, Phys. Rev. Lett. **96**, 077006 (2006).
[8] F. M. F. de Groot and A. Kotani, *Core Level Spectroscopy of Solids* (Taylor & Francis, New York, 2008).
[9] T. E. Westre, P. Kennepohl, J. G. DeWitt, B. Hedman, K. O. Hodgson, and E. I. Solomon, J. Am. Chem. Soc. **119**, 6297 (1997).
[10] F. M. F. de Groot, Chem. Rev. **101**, 1779 (2001).
[11] M.-A. Arrio, S. Rossano, C. Brouder, L. Galoisy, and G. Calas, Europhys. Lett. **51**, 454 (2000).
[12] A. Kotani, K. Okada, G. Vankó, G. Dhalenne, A. Revcolevschi, P. Giura, and A. Shukla, Phys. Rev. B **77**, 205116 (2008).
[13] G. Vankó, F. M. F. de Groot, S. Huotari, R. J. Cava, T. Lorenz, and M. Reuther, arXiv:0802.2744.
[14] J. M. Chen, J. M. Lee, S. W. Huang, K. T. Lu, H. T. Jeng, C. K. Chen, S. C. Haw, T. L. Chou, S. A. Chen, N. Hiraoka, H. Ishii, K. D. Tsuei, and T. J. Yang, Phys. Rev. B **82**, 094442 (2010).
[15] P. Glatzel, A. Mirone, S. G. Eeckhout, M. Sikora, and G. Giuli, Phys. Rev. B **77**, 115133 (2008).

[16]A. Kotani and S. Shin, Rev. Mod. Phys. **73**, 203 (2001).
[17]W. A. Harrison, *Electronic Structure and the Properties of Solids: The Physics of the Chemical Bond* (W. H. Freeman and Company, San Francisco, 1980).
[18]H. K. Mao, J. Xu, V. V. Struzhkin, J. Shu, R. J. Hemley, W. Sturhahn, M. Y. Hu, E. E. Alp, L. Vocadlo, D. Alfè, G. D. Price, M. J. Gillan, M. Schwoerer-Böhning, D. Häusermann, P. Eng, G. Shen, H. Giefers, R. Lübbers, and G. Wortmann, Science **292**, 914 (2001).
[19]T. Gog, G. T. Seidler, D. M. Casa, M. H. Upton, Jungho Kim, S. Stoupin, K. P. Nagle, M. Balasubramanian, R. A. Gordon, T. T. Fister, S. M. Heald, T. Toellner, J. P. Hill, D. S. Coburn, Y.-J. Kim, A. H. Said, E. E. Alp, W. Sutrhahn, H. Yavas, C. A. Burns, and H. Sinn, Synch. Radiat. News **22**, 12 (2009).
[20]R. D. Cowan, *The Theory of Atomic Structure and Spectra* (University of California Press, Berkeley, 1981).
[21]J. van Elp, J. L. Wieland, H. Eskes, P. Kuiper, G. A. Sawatzky, F. M. F. de Groot, and T. S. Turner, Phys. Rev. B **44**, 6090 (1991).
[22]Q. Guo, H. K. Mao, J. Hu, J. Shu, and R. Hemley, J. Phys.: Condens. Matter **14**, 11369 (2002).
[23]Y. Ding, Y. Ren, P. Chow, J. Zhang, S. C. Vogel, B. Winkler, J. Xu, Y. Zhao, and H. K. Mao, Phys. Rev. B **74**, 144101 (2006).
[24]W. J. Duncan, O. P. Welzel, C. Harrison, X. F. Wang, X. H. Chen, F. M. Grosche, and P. G. Niklowitz, J. Phys.: Condens. Matter **22**, 052201 (2010).